Computational Investigation of CO Adsorption and Oxidation on Iron-Modified Cerium Oxide

ARTICLE *in* THE JOURNAL OF PHYSICAL CHEMISTRY C · JULY 2011

Impact Factor: 4.77 · DOI: 10.1021/jp201231d

2 AUTHORS:

Hsin-Tsung Chen
Chung Yuan Christian University
78 PUBLICATIONS **698** CITATIONS
SEE PROFILE

Jee-Gong Chang
National Applied Research Laboratories
109 PUBLICATIONS **1,015** CITATIONS
SEE PROFILE

THE JOURNAL OF PHYSICAL CHEMISTRY C

ARTICLE

pubs.acs.org/JPCC

Computational Investigation of CO Adsorption and Oxidation on Iron-Modified Cerium Oxide

Hsin-Tsung Chen*,† and Jee-Gong Chang‡

†Department of Chemistry, Chung Yuan Christian University, Chungli 32023, Taiwan

‡National Center for High-Performance Computing, No. 28, Nan-Ke Third Road, Hsin-Shi, Tainan, 74147, Taiwan

Supporting Information

ABSTRACT: The mechanisms for the oxidation of CO catalyzed by Fe-modified CeO_2 surfaces have been investigated using periodic density functional theory calculations corrected for the on-site Coulomb interaction by a Hubbard term (DFT + U). The following findings were made: (i) Fe is stable both as an adsorbed atom, $Fe^{\delta+}$ ($\delta < 2$), on the surface and as a dopant, Fe^{3+}, in the surface region. (ii) The Fe dopant facilitates oxygen vacancy formation, whereas Fe adatoms might suppress oxygen vacancy formation. (iii) In addition to physisorbed CO as on the clean surface, physisorbed CO_2 and chemisorbed CO (carbonate, CO_3^{2-}) species are observed on the Fe-doped $CeO_2(111)$ surface. Vibrational frequency calculations were carried to characterize these species. (iv) $CeO_2(111)$ containing positively charged Fe ions, either as supported isolated $Fe^{\delta+}$ adatoms [or small $Fe_x^{\delta+}$ ($x = 2-5$) clusters] or as substitutional Fe^{3+} ions, was found to catalyze the conversion of CO to CO_2. Incorporating Fe^{3+} ions into the ceria lattice as substitutional point defects can instead sustain a full catalytic cycle for CO oxidation and catalyst regeneration. The Fe dopant promotes multiple oxidations of CO without any activation energy, leading to O vacancy formation and CO_2 desorption. Molecular O_2 adsorbs at the O vacancy, forming O adspecies that then drive CO oxidation and recover the stoichiometric Fe-doped CeO_2 surface. A Bader charge analysis was carried to characterize the oxidation state of Fe ions along the catalytic cycle.

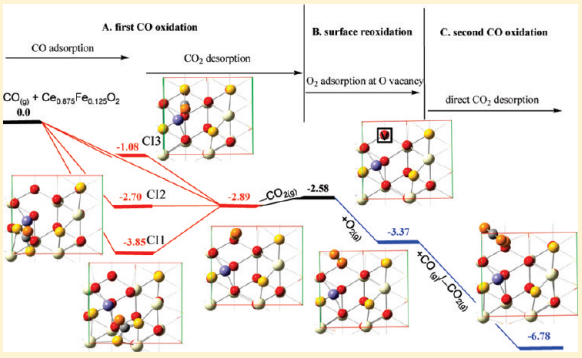

I. INTRODUCTION

Low-temperature CO oxidation is needed in many processes, such as automotive exhaust purification and preferential CO oxidation.[1−4] Metal oxides can be useful catalysts for the CO oxidation. Generally, ceria (CeO_2) is one of the most efficient catalysts because of its unique oxygen storage properties.[5] However, pure ceria cannot satisfactorily fulfill the elevated activity demands for CO oxidation catalysts because of its limited oxygen storage capacity (OSC) and its insufficient thermal stability. Several experimental[6] and theoretical[7−9] studies have demonstrated the surface selectivity for CO oxidation and shown that CO does not adsorb on the stoichiometric $CeO_2(111)$ surface, which is energetically the most stable among the low-index $CeO_2(111)$, (110), and (100) surfaces and represents the largest fraction of the surface exposed on conventional samples. One effective strategy to tackle these problems is to modify ceria with other elements. Shapovalov and Metiu[10] and Camellone and Fabris[11] showed theoretically that the (111) surface of ceria can be made reactive to CO oxidation by doping it with Au. Yang et al.[12] also showed the same behavior on the Cu-doped CeO_2-(111) surface using periodic density functional theory calculations corrected for the on-site Coulomb interaction by a Hubbard term (i.e., DFT + U). Recent studies of Ti-, Zr-, and Hf-doped $CeO_2(110)$ surfaces reported by Nolan[13] and La-doped $CeO_2(111)$ and (110) surfaces reported by Yeriskin and Nolan[14] showed that these surfaces are more reactive to CO adsorption than the undoped surface. The enhancement of ceria for CO oxidation by doping with other metals has also been evidenced by experimental investigations.[15−19]

The reactivity of modified ceria catalysts is controlled by several factors, such as the size of the metal particles, the pretreatment conditions resulting in different morphologies of the catalysts, and the interaction between the added metal and the oxide. As a result, the nature of the active sites on ceria modified with other metals and the reaction mechanisms for CO oxidation are still subjects of debate. Concerning the cost of the catalyst, iron-modified CeO_2 catalysts have been synthesized and characterized by Li et al.,[20] Gupta et al.,[21] and Singh and Hegde,[22] who showed that substitution of Fe in CeO_2 to form $Ce_{1-x}Fe_xO_2$ solid solutions resulted in a high OSC and a high CO oxidation activity at low temperature. The oxidation state of Fe in the iron-modified ceria might play a curial role during the CO oxidation reaction. From an X-ray photoelectron spectroscopy (XPS) study, the presence of Fe^{3+} and Fe^{2+} ions in the iron-modified

Received: February 7, 2011
Revised: June 14, 2011
Published: June 29, 2011

CeO_2 catalysts was identified. However, no metallic Fe^0 ions participated in the reaction.[21,22] The results of temperature-programmed oxidation showed that CO-to-CO_2 conversion utilizes lattice oxygen even though the gas stream does not contain oxygen. This indicates that the reactive oxygen taking part in the oxidation reaction is provided by the ceria. In addition, iron-modified cerium oxide was proposed for the selective oxidation of carbon by Li et al.[23] On the basis of their results, they concluded that the presence of Fe species can enhance the reaction at lower temperatures. Thus, a synergistic electronic interaction between the redox couples Fe^{3+}/Fe^{2+} and Ce^{4+}/Ce^{3+} plays an important role in enhancing the activity of CO oxidation. To the best of our knowledge, no molecular-level study on CO oxidation on iron-modified CeO_2 catalysts is available, although an understanding of the detailed reaction mechanism at the molecular level is vital for the rational design of novel catalysts for low-temperature CO oxidation.

In the present work, we attempted to address CO adsorption and the detailed reaction mechanisms of CO oxidation catalyzed by two model systems, Fe adatoms supported on the $CeO_2(111)$ surface and Fe ions incorporated into $CeO_2(111)$ lattice by replacing Ce ions of the surface. The oxidation states of Fe ions in these catalysts were also characterized. In addition, the step of healing the oxygen vacancies by molecular oxygen was studied to complete a full catalytic cycle for CO oxidation.

This article is organized as follows: The computational details are presented in section II. The calculated results, including the oxygen formation energy of the Fe-doped CeO_2 system, the interaction of Fe adatoms with the stoichometric $CeO_2(111)$ surface, the adsorption of CO on these surfaces, and the relevant mechanisms for CO oxidation, are presented in section III. A brief summary is given in section IV.

II. COMPUTATIONAL METHODS

We applied spin-polarized density functional theory (DFT) plane-wave calculations as implemented in the Vienna ab initio simulation package (VASP) package[24,25] with the projector augmented wave (PAW) method.[26] The generalized gradient approximation (GGA) with the Perdew−Wang 91 (PW91) exchange-correlation functional[27−29] was used. The calculations were carried out using the Brillouim zone sampled with $(3 \times 3 \times 3)$ and $(3 \times 3 \times 1)$ Monkhorst−Pack[30] mesh k-point grids for bulk and surface calculations, respectively, and with a cutoff energy of 400 eV, which allows for convergence to 0.01 eV in the total energy. Because regular DFT methods are unable to describe the localization of the Ce 4f states in the reduced ceria,[31−34] DFT with the Hubbard U term (DFT + U)[35] was applied to accurately correct the strong on-site Coulomb interactions of Ce 4f states.[31−34,36] The issues with regard to the DFT + U method and the selected value of the U parameters have been discussed extensively. However, there is no general rule on a "correct" U value to describe the localized 4f orbitals of Ce. The proposed U values seem to depend on the oxidation states of Ce and the functional used. For example, Loschen et al.[37] proposed a well-balanced U value of 5−6 eV for LDA + U calculations and 2−3 eV for GGA + U calculations. Andersson et al.[38] clarified that the U value must satisfy the criteria of $U > 6$ eV for LDA calculations and $U > 5$ eV for GGA calculations to exactly predict the ground state of Ce_2O_x. As such, we chose $U = 6.3$ eV in the present study.[39−41] In test calculations on the oxygen vacancy formation energy (E_f) for CeO_2 bulk, the calculated E_f value was 3.20 eV with $U = 6.3$ eV, which is very close to the values of 3.15 and 3.19 eV obtained with $U = 5$ and 6.1 eV. In addition, the predicted energy gaps of O 2p → Ce 4f and O 2p → Ce 5d for CeO_2 are 2.4 and 5.5 eV, respectively, which are in better agreement with the experimental values[42−44] of 2.54−3.0 and 6.0 eV, respectively, compared with the DFT results (1.8 and 5.5 eV, respectively).

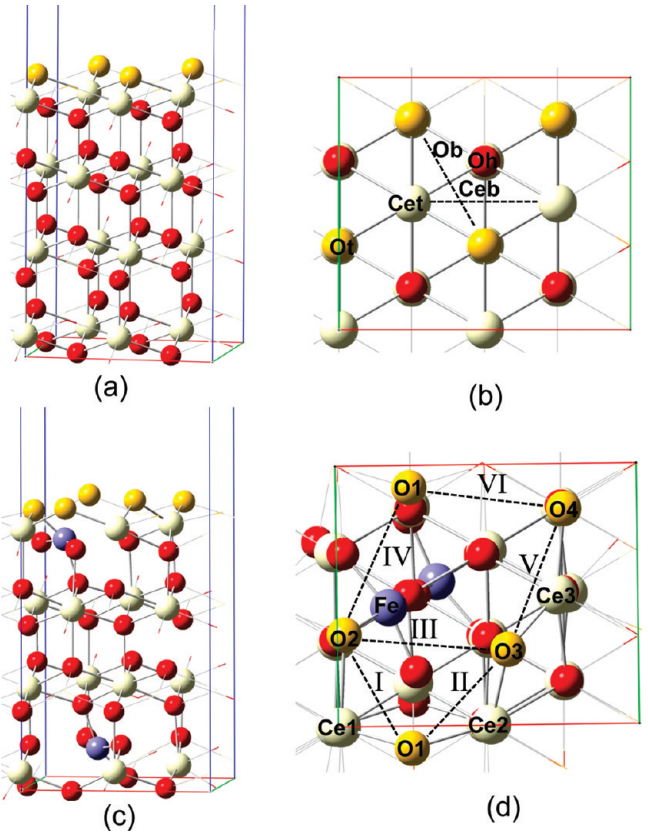

Figure 1. (a) Side and (b) top views of the $CeO_2(111)$ surface. Cet, Ceb, Ot, Ob, and Oh, correspond to Ce top, Ce bridge, O top, O bridge, and O hollow active sites, respectively. (c) Side and (d) top views of the $Ce_{0.875}Fe_{0.125}O_2(111)$ surface model. I, II, III, IV, V, and VI correspond to O1−O2 short, O1−O3 short, O2−O3 long, O1−O2 long, O3−O4 long, and O3−O4 long active sites, respectively. Yellow, red, white, and purple spheres represent the top-layer O, O, Ce, and Fe atoms, respectively. The rectangle represents the supercell used in this study.

Ceria doped with 12.5% Fe, $Ce_{0.875}Fe_{0.125}O_2$, which was found to exhibit a high OSC value,[21,22] was modeled by introducing Fe-doping atoms to substitute Ce atoms in the supercell. The reduced systems were created by removing one oxygen atom, resulting in an oxygen vacancy concentration of 6.25%. For the surface model, we examined only the (111) surface to characterize the CO−$Ce_{0.875}Fe_{0.125}O_2$ interactions because the (111) surface is energetically the most stable[45−47] among the low-index $CeO_2(111)$, (110), and (100) surfaces. As shown in Figure 1, CeO_2 and $Ce_{0.875}Fe_{0.125}O_2(111)$ surface models with 12 atomic layers—a $p(\sqrt{3} \times 2)$ lateral cell—was constructed. The bottom six layers of the surface model were fixed to the estimated bulk parameters, and the remaining layers were fully optimized. A vacuum space greater than 15 Å was introduced to prevent interactions between slabs. The adsorption energies were calculated as $\Delta E_{ads} = E(\text{surface−adsorbate}) - E(\text{surface}) - E(\text{adsorbate})$, where $E(\text{surface−adsorbate})$, $E(\text{surface})$, and

dx.doi.org/10.1021/jp201231d | J. Phys. Chem. C 2011, 115, 14745–14753

Table 1. Lattice Constants and O Vacancy Formation Energies (E_f) of CeO_2 and $Ce_{0.875}Fe_{0.125}O_2$ Materials

	lattice constants (Å)			E_f (eV)	
species	unreduced	reduced	vacancy position	bulk	surface
CeO_2	5.45 (5.41)[a]	5.50		3.20	2.08
$Ce_{0.875}Fe_{0.125}O_2$	5.42	5.46 (5.42)[a]	VO1[b]	1.04, 1.48[d]	0.71
			VO2		1.11
			VO3		0.68
			VO4		1.84
			V*(O1)[c]		1.64

[a] Values in parentheses are experimental data. [b] Labeling of the O atoms is shown in Figure 1d. VO1 means that O1 has been removed, and so on. [c] Second vacancy after VO3. [d] Different formation energies calculated from the different coordination shells of the Fe—O bond.

E(adsorbate) are the calculated electronic energies of adsorbed species on the surface, the bare surface, and the adsorbate in the gas phase, respectively. The climbing image nudged elastic band (CI-NEB) method[48,49] was applied to map out minimum-energy paths (MEPs) after locating plausible local minima. All transition states were verified by the number of imaginary frequencies (NIMG) with NIMG = 1. The charge-density difference was calculated using the expression: $\Delta\rho_{diff} = \rho$(surface + adsorbate) — ρ(surface) — ρ(adsorbate), where ρ(surface + adsorbate), ρ(surface), and ρ(adsorbate) are the charge densities of adsorbed species on the surface, the bare surface, and the adsorbate, respectively.

III. RESULTS AND DISCUSSION

III.A. Fe-Doped $Ce_{0.875}Fe_{0.125}O_2$ Bulk and Surface. The geometries of stoichiometric and reduced bulk $Ce_{0.875}Fe_{0.125}O_2$ were optimized at GGA + U levels with and without considering spin polarization. One should note that the external (cell volume and cell shape) and internal (atomic ions and lattice parameters) degrees of freedom were allowed to relax until forces and stress vanished in the bulk calculations. To avoid the Pulay stress and related problems, we restarted the calculations several times using a larger cutoff energy, ENCUT = 1.3 × 400 eV, and a very highly accurate energy with the PREC = High command. The predicted lattice constant of bulk $Ce_{0.875}Fe_{0.125}O_2$ is 5.42 Å, whereas that for bulk CeO_2 is 5.45 Å. The theoretical values are close to the experimental values of 5.41[43] and 5.42[21] Å for bulk CeO_2 and $Ce_{0.875}Fe_{0.125}O_2$, respectively. The optimized Ce_8O_{16} unit has all Ce—O bond lengths equal to 2.36 Å. Optimized $Ce_{0.875}Fe_{0.125}O_2$ shows geometric distortions of the oxygen lattice with shorter and longer Ce—O bond averages of 2.26 and 2.48 Å, respectively, and shorter and longer Fe—O bond averages of 1.79 and 2.84 Å, respectively. Introduction of the O vacancy gives rise to significant distortions of the oxygen lattice, as the Ce—O bonds are distributed over the range of 2.29−2.44 Å and the Fe—O bonds are distributed over the range of 1.92−3.00 Å.

Oxygen vacancy formation is described by the reaction $Ce_{1-x}M_xO_2 \rightarrow Ce_{1-x}M_xO_{2-\delta} + {}^1/_2O_2$.[50] The oxygen vacancy formation energy, E_f, was computed according to the equation

$$E_f = E(Ce_{1-x}M_xO_{2-\delta}) + \frac{1}{2}E(O_2) - E(Ce_{1-x}M_xO_2) \quad (1)$$

where $E(Ce_{1-x}M_xO_2)$ indicates the energy of the bulk or surface $Ce_{1-x}M_xO_2$, $E(O_2)$ is the energy of gas-phase O_2, and $E(Ce_{1-x}M_xO_{2-\delta})$ is the energy of the bulk in the presence of one oxygen vacancy. The E_f value of $Ce_{0.875}Fe_{0.125}O_2$ was calculated as 1.05 and 1.48 eV depending on the different coordination shells of the Fe—O bond. Compared to CeO_2 and $Ce_{0.875}Zr_{0.125}O_2$, the smaller E_f value for $Ce_{0.875}Fe_{0.125}O_2$ (1.05 versus 3.20 for CeO_2 and 2.03 eV for CeO_2 and $Ce_{0.875}Zr_{0.125}O_2$) indicates that $Ce_{0.875}Fe_{0.125}O_2$ exhibits a higher OSC than CeO_2 and $Ce_{0.875}Zr_{0.125}O_2$, which is consistent with the experimental results.[21]

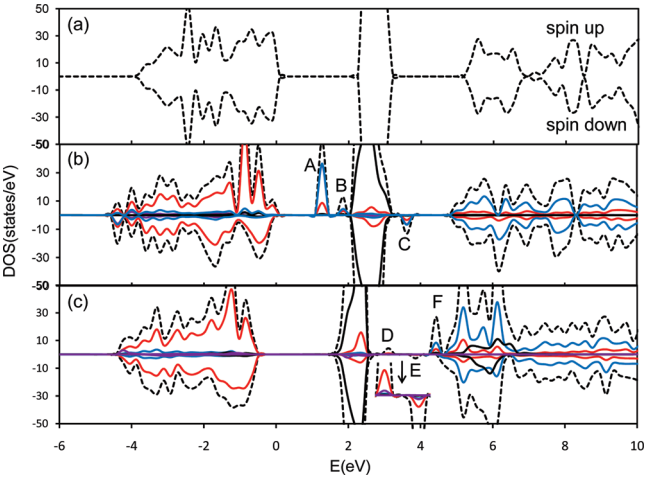

Figure 2. Density of states and local density of states for (a) the CeO_2(111) surface, (b) the $Ce_{0.875}Fe_{0.125}O_2$(111) surface, and (c) a single Fe atom adsorbed at the hollow site of the CeO_2(111) surface. The black dashed, black solid, blue, red, and purple lines represent the total, Ce(f), Ce(d), O(p), and Fe(d) densities of states, respectively. The energy at E = 0 eV represents the Fermi energy.

The relaxed structure of the Fe-doped $Ce_{0.875}Fe_{0.125}O_2$(111) surface in which two Ce atoms are replaced by two Fe atoms is shown in Figure 1c. In this structure, the Fe atom has relaxed to form four short Fe—O bonds of 1.83 Å on average and two long Fe—O bonds of 2.93 Å on average. The length of the short Fe—O bonds (1.83 Å) is close to that of the Fe—O bonds in γ-Fe_2O_3 (1.89 Å).[51] The surface O vacancy formation was calculated as shown in Table 1. The formation energies of the various nonequivalent surface oxygen atoms of the top layer were calculated as 0.68, 1.11, 0.71, and 1.84 eV. The nearest-neighbor oxygen anions (O1, O2, and O3; see Figure 1d) to Fe cations have much smaller formation energies than the undoped CeO_2(111) surface (2.08 eV), indicating that O vacancy formation is very much facilitated by Fe doping. The formation of a second oxygen vacancy from the O1 site on the optimized surface, with an O vacancy at the O3 site already present [denoted as V*(O1)], also needs less energy, with

dx.doi.org/10.1021/jp201231d | J. Phys. Chem. C 2011, 115, 14745–14753

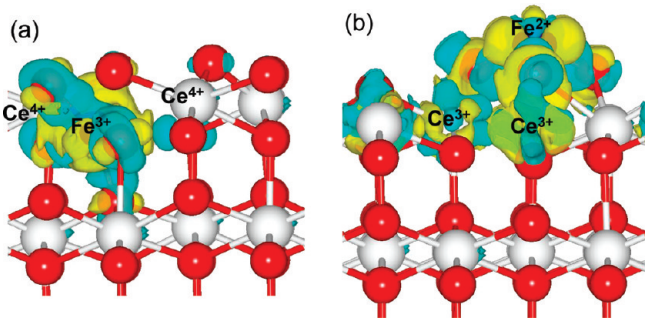

Figure 3. Illustration of charge-density difference for (a) the $Ce_{0.875}Fe_{0.125}O_2(111)$ surface and (b) a single Fe atom adsorbed at the hollow site of the $CeO_2(111)$ surface. $\Delta\rho_{diff}$ isosurfaces were calculated at 0.05 $bohr^{-3}$. The values are effective charges that were calculated by the Bader analysis program.

an E_f value of 1.64 eV. Although it is more difficult to make the second vacancy than the first, the vacancy formation energy is still much smaller than that of the pure surface. Thus, the Fe dopant might serve as the seed for the formation of oxygen vacancy clusters on ceria surfaces.

The stoichiometric $CeO_2(111)$ system is known to be an insulator, and the features of the electronic density of states (DOS) shown in Figure 2a are in good agreement with previous DFT + U results.[12] We found three new features in the band gap, labeled A−C (Figure 2b), that are contributed from the overlap between the Fe(d) states and the O(p) states, resulting in Fe—O binding. Interestingly, no Ce(f) state was found in the band gap, indicating that no Ce^{4+} reduces to Ce^{3+}. This is corroborated by the Bader charge calculations, which were carried out to characterize the oxidation states in bulk and surface $Ce_{0.875}Fe_{0.125}O_2$. The Bader charges of Fe and Ce in the stoichiometric bulk and surface were calculated to be 6.15−6.21 e and ∼9.6 e, which are close to those of γ-Fe_2O_3 (6.35 e) and CeO_2 (9.60 e). Accordingly, in both cases, the oxidation states for Fe and Ce are characterized as 3+ and 4+. This was verified by a charge-density difference calculation, as shown in Figure 3. For the reduced ceria, the Fe neighboring the O vacancy was still in the 3+ oxidation state (the Bader charge was between 6.12 and 6.26 e), whereas the Ce^{4+} ion neighboring the O vacancy was reduced to Ce^{3+} (the Bader charge was 9.90 e).

III.B. Fe/CeO_2(111) Surface. Plausible intermediates for the Fe−CeO_2 interactions were initially optimized by placing a single Fe atom at different active sites on the (111) surface, including Ce top, O top, Ce−Ce bridge, O−O bridge, and O hollow, corresponding to Cet, Ot, Ceb, Ob, and Oh, respectively, as illustrated in Figure 1b. All optimized structures are presented in Figure S1. Table 2 lists the relative adsorption energies and the calculated Bader charge of the Fe atom in these configurations. In all cases, the interactions between the Fe atom and the stoichiometric $CeO_2(111)$ surface, including charge transfer from the Fe atom to the surface, yield the reduction of Ce ions. The most stable adsorption site for an Fe adatom was found to be the O-hollow site. The calculated adsorption energy and the Fe—O distance are −5.43 eV and 1.84 Å, respectively. The Bader charge analysis reveals that ∼1.50 e is transferred from the metal to the oxide, resulting in the formation of a positively charged $Fe^{\delta+}$ ion with an oxidation state of 2+. As shown in Figure 3b, the excess charge in the oxide is mostly localized around the surface O atoms bound to Fe and on the Ce^{4+} ions, which reduce to Ce^{3+}.

Table 2. Adsorption Energies (E_{ads}) of an Fe Adatom on the Stoichiometric $CeO_2(111)$ Surface, as Well as on O and Ce Vacancies and the Calculated Bader Charges of the Fe Atom in These Configurations[a]

adsorption site	E_{ads} (eV)	Fe
Ce top	−3.98	6.53(Fe^{2+})
Ce bridge	−2.68	7.41($Fe^{\delta+}$)
O top	−1.74	7.52($Fe^{\delta+}$)
O bridge	−4.34	6.92($Fe^{\delta+}$)
O hollow	−5.43	6.50(Fe^{2+})
V_o	−0.63	8.09($Fe^{\delta-}$)
O hollow (V_o)	−4.17	7.01($Fe^{\delta+}$)
V_{Ce}	−11.36	6.17(Fe^{3+})

[a] Calculated Bader charges of Fe in FeO and Fe_2O_3 are 6.60 and 6.35 e, respectively.

This is verified by the calculated DOS, which displays three new features in the band gap, labeled D−F (Figure 2c). The local DOS analysis indicates that states D and E are related to the Fe—O bonding resulting from the overlap between the Fe d states and the O p states. The state F close to the conduction band and the states at 5−7 eV (black solid line in Figure 2c) result in the charge transferred from Fe to the substrate and localized on the Ce f states, leading to the $Ce^{4+} \rightarrow Ce^{3+}$ reduction. The vacancy formation energy of the Fe/CeO_2 system was calculated to be 3.34 eV by removing one of the three equivalent nearest-neighbor surface O atoms bound to Fe atom. This value is larger than that for pure $CeO_2(111)$, suggesting that Fe adsorption on the $CeO_2(111)$ surface might suppress O vacancy formation.

In addition, the Fe adsorbed at the O vacancy site of the partially reduced $CeO_{2-x}(111)$ surface was also studied. The adsorption energy was found to be −0.63 eV, which is much larger than those for an Fe atom adsorbed on the stoichiometric CeO_2-(111) surface, indicating that the Fe atom is not likely to occupy an O lattice site. The Bader charge analysis revealed that ∼0.1 e is transferred from the oxide to the metal, resulting in the formation of a negatively charged $Fe^{\delta-}$ ion. The adsorption energy of an Fe atom adsorbed at the O-hollow site on the partially reduced $CeO_{2-x}(111)$ surface was calculated to be −4.17 eV. It turns out that the Fe atom prefers to localize at the O-hollow site even on the partially reduced $CeO_{2-x}(111)$ surface. According to the Bader charge analysis, the two excess electrons created by O vacancy formation give rise to a significant charge transfer (0.5 e) from the oxide surface to the Fe atom while the remaining 1.5 e is mainly transferred to the three Ce ions in the second atomic layer of the surface. However, the adsorbed Fe atom still remains positive charge in the Fe/CeO_{2-x} system, except for the Fe adsorbed at the O vacancy (see Table 2).

III.C. CO Adsorption and Oxidation on the Fe/CeO_2(111) and $Ce_{0.875}Fe_{0.125}O_2$(111) Surfaces. Only weak physisorption of CO on the stoichiometric $CeO_2(111)$ surface was found (see Table 3). This result is consistent with the previous studies reported by Huang and Fabris,[7] Nolan and Watson,[8] and Yang et al.[9] In the present work, we explored whether iron-modified ceria changes this behavior. To this end, we studied the interaction of a CO molecule with Fe/$CeO_2(111)$ and $Ce_{0.875}Fe_{0.125}O_2(111)$ surfaces.

III.C.1. CO Adsorption and Oxidation on the Fe/CeO_2(111) Surface. The adsorption of a CO molecule on an Fe adatom in the lowest-energy O-hollow site was studied. As shown in

Table 3. Adsorption Energies (E_{ads}) and Calculated Frequencies of a CO Molecule on the Stoichiometric $CeO_2(111)$, $Ce_{0.875}Fe_{0.125}O_2(111)$, and $Fe/CeO_2(111)$ Surfaces[a]

	CeO_2		$Ce_{0.875}Fe_{0.125}O_2$		Fe/CeO_2	
adsorption site	E_{ads} (eV)	frequency (cm^{-1})	E_{ads} (eV)	frequency (cm^{-1})	E_{ads} (eV)	frequency (cm^{-1})
			Physisorption			
Ce1 top	−0.17	2133	−0.23	2154		
Ce2 top			−0.19	2152		
Ce3 top			−0.19	2158		
Fe top			−0.01	2099	−0.54	1977
O4 top	0.08	2131	−0.04	2155	−0.70	2052
O1−O4 long			−0.18	2136		
O2−O3 long			−0.15	2074		
O3−O4 long			−0.14	2120		
			Chemisorption			
O1−O2 short			−2.70	1755		
O1−O3 short			−3.85	1720		
O1−O2 long			−1.08	1904		
			CO_2 Formation			
O1 top			−2.89	2391, 1331, 626		
O2 top			−2.62	2393, 1329, 623		
O3 top			−2.80	2386, 1329, 630		

[a] Calculated frequencies are 2136 cm^{-1} for a gas-phase CO molecule and 2377, 1321, and 644 cm^{-1} for a gas-phase CO_2 molecule.

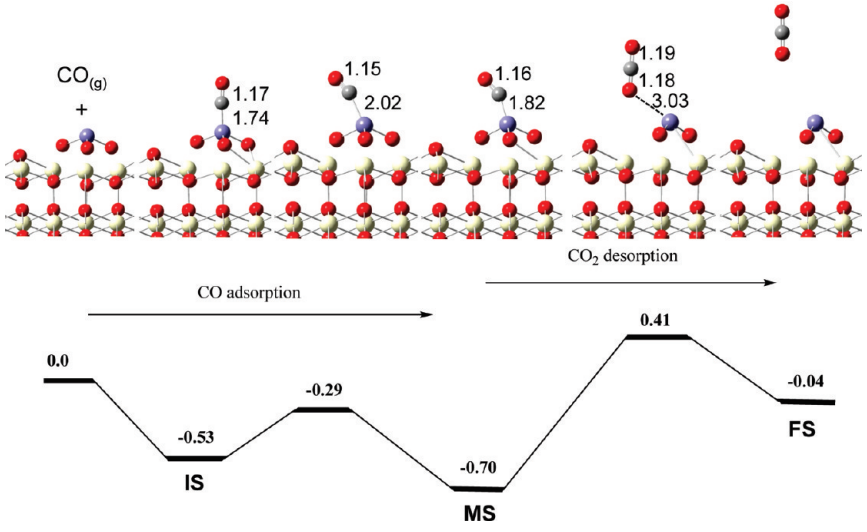

Figure 4. Calculated reaction mechanism and corresponding energies for CO oxidation catalyzed by a supported Fe atom adsorbed at the hollow site of the $CeO_2(111)$ surface. The relevant bond lengths indicated in the top panel are expressed in angstroms, and the relative energies in the potential energy diagram are expressed in electronvolts.

Figure 4, two stable configurations (**IS** and **MS**) with the CO bond to the surface Fe adatom were found: one is perpendicular to the surface, and the other tilts with respect to the surface. The adsorption energies were calculated as −0.53 and −0.70 eV, respectively. The C—O bond lengths of the adsorbed CO molecule were found to be 1.17 and 1.16 Å, essentially unaffected with respect to the calculated value (1.14 Å) of the CO gas phase; the Fe−C distances were calculated as 1.74 and 1.82 Å. However, CO adsorption on the $Fe/CeO_2(111)$ surface becomes stronger than that on the pure $CeO_2(111)$ surface (see Table 3).

The oxidation of CO catalyzed by $Fe/CeO_2(111)$ has been addressed, and the calculated reaction mechanism is illustrated in Figure 4. First, the CO adsorbs at the Fe adatom to form **IS** with an exothermicity of 0.53 eV. The **IS** isomerizes to **MS**, in which the CO tilts from the surface, with a slight barrier of 0.24 eV. Then, the adsorbed CO is oxidized by a lattice oxygen atom, leading to CO_2 desorption and O vacancy formation. This process is the rate-limiting step of the overall reaction with a barrier of 1.11 eV. The overall reaction is exothermic by only about 0.04 eV. During the oxidation, the Fe adatom receives

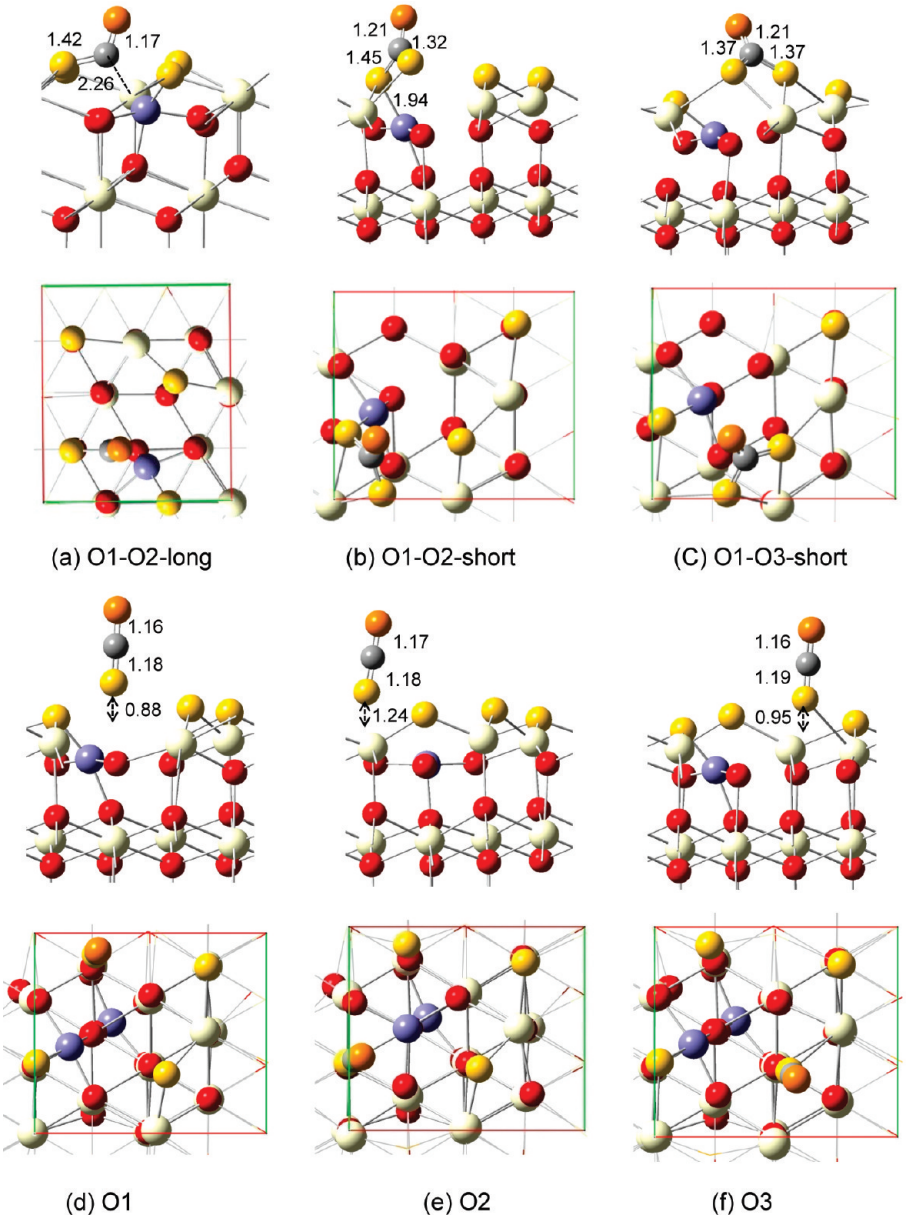

Figure 5. Side and top views of the optimized structures of CO chemisorption and CO_2 formation on the $Ce_{0.875}Fe_{0.125}O_2(111)$ surface. CO chemisorption: (a) O1−O2 long, (b) O1−O2 short, (c) O1−O3 short. CO_2 formation: (d) O1, (e) O2, (f) O3.

~0.5 e from the surface and still remains positively charged ($Fe^{\delta+}$). This is consistent with the experimental observation[21] that no Fe^0 is detected.

The size of the metal cluster is one of the factors for controlling the activity of these catalysts. To this end, we considered the case of a small Fe_x (x = 2−5) cluster adsorbed on ceria, whose calculated structure is depicted in Figure S2 of the Supporting Information. The adsorption energy of Fe on $Fe_{x-1}/CeO_2(111)$ system was calculated to be between −1.95 and −4.15 eV (see Table S1, Supporting Information), indicating that even Fe species such as $Fe^{\delta-}$ favor the aggregation of further Fe adatoms. It should be noted that, in the case of an Fe_2 dimer adsorbed on an O vacancy, the Fe_2 dimer reveals a positively charged $Fe_2^{\delta+}$ moiety when a second Fe atom binds to the $Fe^{\delta-}/CeO_{2-\delta}(111)$ system. However, the CO molecule strongly binds to the Fe_x cluster with an adsorption energy of between −2.26 an −1.36 eV (see Table S2, Supporting Information) compared to the case of $Fe/CeO_2(111)$ system, indicating that CO oxidation is enhanced by cluster sizes as small as Fe_2 .

III.C.2. CO Adsorption and Oxidation on the $Ce_{0.875}Fe_{0.125}O_2$-(111) Surface. To describe the interactions between a CO molecule and the $Ce_{0.875}Fe_{0.125}O_2(111)$ surface, a CO molecule was placed at various sites on the $Ce_{0.875}Fe_{0.125}O_2(111)$ surface, including Ce top, O top, Fe top, and O−O bridge, as seen in Figure 1d. The interactions can be divided into three types of adsorption when the (111) surface has been doped with Fe: CO physisorption, CO chemisorption, and CO_2 physisorption. The optimized configurations of CO chemisorption and CO_2 physisorption are depicted in Figure 5, and the structures of CO physisorption are displayed in Figure S3 (Supporting Information). The adsorption energies of all optimized configurations are reported in Table 3.

dx.doi.org/10.1021/jp201231d |*J. Phys. Chem. C* 2011, 115, 14745–14753

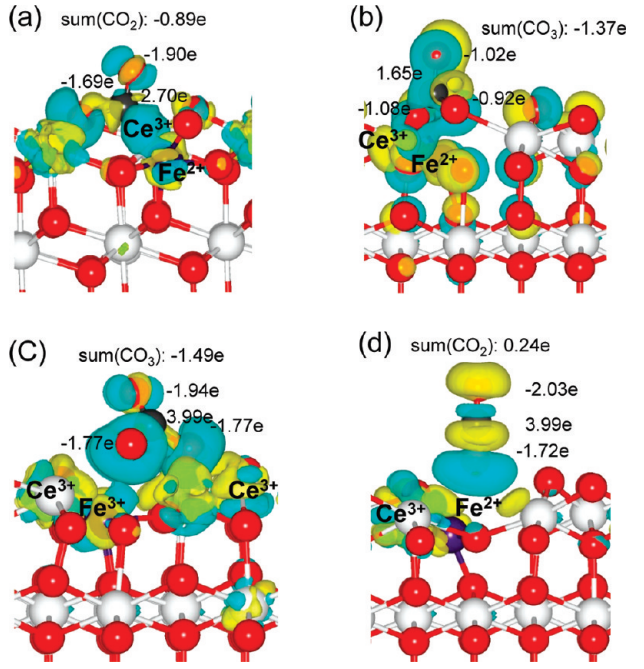

Figure 6. Illustration of the charge-density difference for CO oxidation on the $Ce_{0.875}Fe_{0.125}O_2(111)$ surface: (a) **CI3** (O1−O2 long), (b) **CI2** (O1−O2 short), (c) **CI1** (O1−O3 short), (d) product (O1). $\Delta\rho_{diff}$ isosurfaces were calculated at 0.05 $bohr^{-3}$. The values are effective charges that were calculated with the Bader analysis program.

CO physisorption was observed at the Ce, Fe, and O4 top sites, as well as at the long O-bridge sites (O1−O4 long, O2−O3 long, and O3−O4 long). As shown in Table 3, the adsorption energies are between −0.01 and −0.23 eV, which is close to that for CO physisorption on the $CeO_2(111)$ surface. Unlike for the CeO_2 and $Fe/CeO_2(111)$ surfaces, CO chemisorption was found to occur at the short O-bridge (O1−O2 short and O1−O3 short) and Fe−O1 sites. The adsorbed CO binds to two surface oxygen ions, forming a carbonate-like species with the CO tilting from the surface. The adsorption energies for the two carbonate-like species are −2.70 and −3.85 eV. The C—O and $C—O_{surf}$ bond distances are 1.21 and 1.32−1.45 Å, respectively, which are elongated compared to that in a free CO molecule (1.18 Å). A Bader charge analysis gives net charges of −1.37 and −1.49 e (see Figure 6) for the two carbonate-like species, which seem to be reasonable values for a bound CO_3^{2-} ion. The other chemisorbed CO was bound to the surface Fe and O1 ions with an adsorption energy of −1.08 eV. The C—O, $C—O_{surf}$, and C—Fe bond distances were found to be 1.17, 1.42, and 2.26 Å, respectively. Interestingly, a CO molecule placed at the top of surface O1, O2, and O3 ions neighboring the substitutional Fe^{3+} ion led to the formation of CO_2 floating on the surface with an oxygen vacancy left in the surface. The process releases between −2.62 and −2.82 eV. The nature of the adsorbed CO_2 species is similar to that of a free CO_2 molecule, with C—O bond distances close to 1.20 Å and an O—C—O angle of almost 180°. In view of the interactions between a CO_2 molecule and the reduced $Ce_{0.875}Fe_{0.125}O_2(111)$ surface, the CO_2 molecule is weakly bound to the surface with the desorption energies of between −0.18 and −0.44 eV.

The reaction mechanisms for CO oxidation and catalyst regeneration are depicted in Figure 7 and consist of three steps: (A) oxidation of a first CO molecule on the stoichiometric $Ce_{0.875}Fe_{0.125}O_2(111)$ surface through participation of a lattice oxygen, leading to O vacancy formation and CO_2 desorption (Figure 7A); (B) adsorption of molecular O_2 at the O vacancy, leading to the formation of surface O adspecies (Figure 7B); and (C) interaction of a CO molecule with these O adspecies, which drives CO oxidation and regeneration of the stoichiometric $Ce_{0.875}Fe_{0.125}O_2$ surface (Figure 7C). Two reaction pathways of the first CO oxidation were considered, namely, the Langmuir−Hinshelwood (LH) and Eley−Rideal (ER) mechanisms, as shown in Figure 7. The LH mechanism starts from adsorption of CO with adsorption energies of −3.85, −2.70, and −1.08 eV, forming carbonate-like intermediates, **CI1**, **CI2**, and **CI3**, respectively. By breaking one C—O bond in the **CI1** and **CI2** intermediates, the reactions go to the adsorption of CO_2 with endothermicities of 0.95 and 0.19 eV, respectively, whereas breaking the Fe—C bond of **CI3** to form CO_2 adsorption is exothermic by 1.81 eV. The ER mechanism can take place directly by abstracting the surface oxygen ions neighboring the substitutional Fe^{3+} ion and leads to the formation of CO_2. The process releases −2.89 eV. The desorption of CO_2 with the formation of a surface O vacancy and reduction of the neighboring Ce^{4+} ion to Ce^{3+} requires only 0.31 eV. On the basis of Bader charge population analysis (see Figure 6), we interpret the Fe ion as Fe^{2+} along the most probable mechanism of CO oxidation through the intermediates **CI2** and **CI3**. In addition, we also considered second oxidation by the ER mechanism on the reduced substrate after the release of the oxidation of a CO molecule. The second oxidation has no activation barrier, is less exothermic (−2.43 eV) than the first one, and results in the formation of a second O vacancy neighboring the Fe ion. The reduced catalysts can be sealed by an O_2 molecule from the gas phase. The adsorption energy of the O_2 molecule on the O vacancy was calculated to be −0.79 eV. The O—O bond length has increased from the O_2 gas-phase value of 1.21 to 1.35 Å, and the Ce^{3+} ion of the surface reoxidized to Ce^{4+}. The resulting O adspecies are active and can promote the direct oxidation of a CO molecule, leading to the formation of CO_2, which desorbs without any activation barrier and is exothermic by 3.41 eV (see Figure 7C). The Bader charge analysis for the CO oxidation and catalyst regeneration through healing of the vacancy by molecular O_2 on the $Ce_{0.875}Fe_{0.125}O_2(111)$ surface shows a catalytic cycle in which the positive oxidation state of the substitutional Fe ion is preserved throughout the reaction.

III.C.3. Vibrational Spectra Calculations. In addition to the mechanistic studies, to guide a future surface vibrational spectroscopic study, the vibrational frequencies for the adsorbed species on the Fe/CeO_2 and $Ce_{0.875}Fe_{0.125}O_2(111)$ surface were estimated as summarized in Table 3. The calculated frequencies of 1977 and 2052 cm^{-1} for CO adsorbed on the $Fe/CeO_2(111)$ surface are assigned to linearly bonded CO on Fe and to CO adsorbed on the Fe−ceria interface, respectively, and are similar to those on Pt/CeO_2 catalyst (1970−1960 and 2054 cm^{-1}).[52] For CO on the $Ce_{0.875}Fe_{0.125}O_2(111)$ surface, the predicted vibrational frequencies in the range of 2074−2158 cm^{-1} are attributed to the C—O stretching of CO physisorption in which the values are close to that of a gas-phase CO molecule (2136 cm^{-1}). On the other hand, the predicted C—O frequencies of carbonate-like species (1720 and 1755 cm^{-1}) are in close agreement with the experimental value,[53,54] 1728 cm^{-1}. The strong red shifts of approximately −400 cm^{-1} with respect to the values of a gas-phase CO molecule are consistent with the

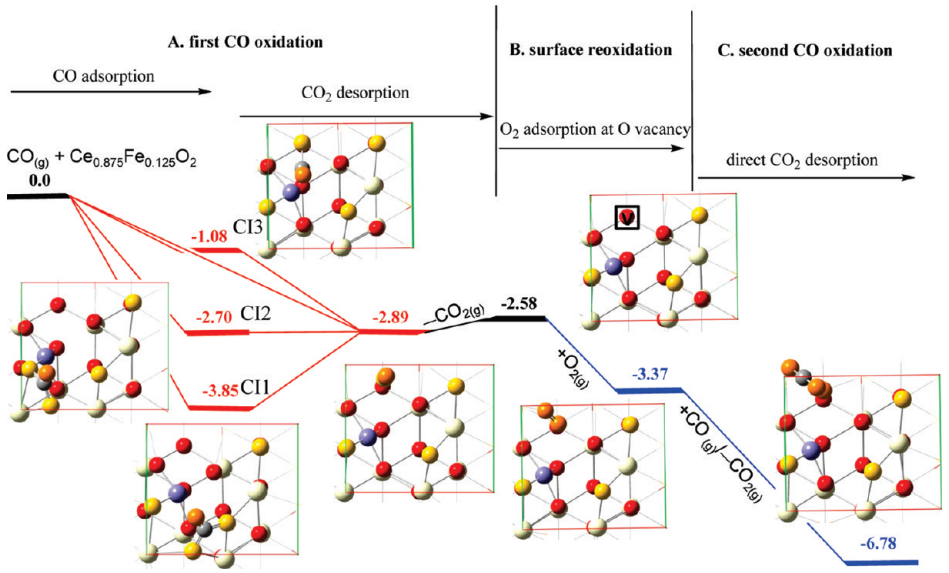

Figure 7. Calculated potential energy diagram for CO oxidation on $Ce_{0.875}Fe_{0.125}O_2$ and catalyst regeneration. The proposed catalytic cycle involves (A) oxidation of a first CO molecule on the stoichiometric $Ce_{0.875}Fe_{0.125}O_2(111)$ surface through participation of a lattice oxygen atom, leading to O vacancy formation and CO_2 desorption; (B) adsorption of molecular O_2 at the O vacancy, leading to the formation of surface adspecies; and (C) interaction of a CO molecule with these O adspecies, which drives CO oxidation and regeneration of the stoichiometric $Ce_{0.875}Fe_{0.125}O_2$ surface.

observation in experiments for ceria powder with carbonate species and in theoretical calculations for $CeO_2(110)$ surface by Yang et al.[50] and Herschend et al.[55] The vibrational mode of CO chemisorption at 1904 cm^{-1} is assigned to linearly bonded CO on the Fe−ceria interface. The estimated vibrational frequencies for the antisymmetric stretching mode, symmetric stretching mode, and bending mode of the adsorbed CO_2 species are in the ranges of 2386−2393, 1329−1331 and 623−630 cm^{-1}, respectively (see Table 3). Compared to the values for a gas-phase CO_2 molecule (2377, 1321, and 644 cm^{-1}), the frequency shifts of the adsorbed CO_2 species are very small, indicating and confirming that, indeed, the new adsorption species is likely a weakly adsorbed CO_2 species.

IV. CONCLUSIONS

In conclusion, we have provided insight into the interactions of CO with the Fe-doped $CeO_2(111)$ surface, as well as the catalytic mechanisms for CO oxidation, using periodic DFT + U calculations. Our calculations show that Fe is stable both as an adsorbed atom $Fe^{\delta+}$ ($\delta < 2$) on the surface and as a dopant (Fe^{3+}) in the surface region. The Fe^{3+} dopant in ceria leads to strong structural distortions and smaller oxygen vacancy formation energies compared to the undoped system. In contrast, $Fe^{\delta+}$ ($\delta < 2$) adsorption on the stoichiometric $CeO_2(111)$ surface might suppress oxygen vacancy formation. Isolated Fe adatoms supported by stoichiometric $CeO_2(111)$ surfaces were found to induce charge redistribution at the $Fe/CeO_2(111)$ contact, leading to the reduction of the ceria substrate (Ce^{3+}) and surface $Fe^{\delta+}$ ($\delta < 2$). Physisorbed CO, physisorbed CO_2, and chemisorbed CO (carbonate, CO_3^{2-}) species were observed on the Fe-doped $CeO_2(111)$ surface; in contrast, on the clean ceria-(111) surface, only physisorbed CO was previously observed. Furthermore, the vibrational frequencies of the adsorbed CO species were estimated to guide future surface vibrational spectroscopic studies. The oxidation of CO catalyzed by Fe/CeO_2-(111) was addressed and found to be controlled by CO_2 desorption with a high barrier of 1.11 eV. In addition, we have provided evidence that the activity toward CO oxidation by Fe nanoparticles can be enhanced for small clusters [Fe_x ($x = 2-5$)] because of the higher CO adsorption energy. Incorporating Fe^{3+} ions into the ceria lattice as substitutional point defects can instead sustain a full catalytic cycle for CO oxidation and catalyst regeneration consisting of three steps: Fe cations in the Fe-doped CeO_2 surface promote multiple oxidations of CO without any activation energy, leading to O vacancy formation and CO_2 desorption. Molecular O_2 adsorbed at the O vacancy results in the formation of surface O adspecies that then drive CO oxidation and regeneration of the stoichiometric Fe-doped CeO_2 surface. On the basis of Bader charge population analysis, the substitutional Fe ions retain the positive oxidation state along the catalytic cycle, thus preventing the deactivation of Fe-doped CeO_2 catalysts under operating conditions. These results rationalize the experimental observation[22] that $Ce_{1-x}Fe_xO_{2-\delta}$ shows a higher OSC and higher percentages of CO oxidation at lower temperature.

■ ASSOCIATED CONTENT

Supporting Information. Adsorption energies (E_{ads}) of an Fe adatom and a CO molecule on the $Fe_{x-1}/CeO_2(111)$ system and sums of the calculated effective Bader charges of the Fe clusters for these configurations (Tables S1 and S2). Optimized geometries of adsorbed Fe species at various sites on the $CeO_2(111)$ surface (Figure S1) and adsorbed CO species on Fe_x ($x = 2-5$)/$CeO_2(111)$ (Figure S2), as well as optimized configurations of CO physisorption on the $Ce_{0.875}Fe_{0.125}O_2$-(111) surface (Figure S3). This material is available free of charge via the Internet at http://pubs.acs.org.

■ AUTHOR INFORMATION

Corresponding Author
*E-mail: htchen@cycu.edu.tw.

■ ACKNOWLEDGMENT

We are grateful to (1) the National Science Council, Republic of China, under Grant NSC 99-2113-M-492-001-MY2, and the Taiwan National Center for Theoretical Sciences (NCTS) for financial support and (2) the National Center for High-Performance Computing, Taiwan, for the computer time and facilities.

■ REFERENCES

(1) Bourane, A.; Bianchi, D. *J. Catal.* **2001**, *202*, 34.
(2) Bunluesin, T.; Gorte, R. J.; Graham, G. W. *Appl. Catal. B* **1997**, *14*, 105.
(3) Gamarra, D.; Belver, C.; Fernández-Garcia, M.; MartÚnez-Arias, A. *J. Am. Chem. Soc.* **2007**, *129*, 12064.
(4) Pozdnyakova, O.; Teschner, D.; Wootsch, A.; Kröhnert, J.; Steinhauer, B.; Sauer, H.; Toth, L.; Jentoft, F. C.; Knop-Gericke, A.; Paal, Z.; Schlogl, R. *J. Catal.* **2006**, *237*, 1.
(5) Trovarelli, A. *Catalysis by Ceria and Related Materials*; Imperial College Press: London, 2002.
(6) Aneggi, E.; Llorca, J.; Boaro, M.; Trovarelli, A. *J. Catal.* **2005**, *234*, 88.
(7) Huang, M.; Fabris, S. *J. Phys. Chem. C* **2008**, *112*, 8643.
(8) Nolan, M.; Watson, G. W. *J. Phys. Chem. B* **2006**, *110*, 16600.
(9) Yang, Z.; Woo, T. K.; Baudin, M.; Hermansson, K. *J. Chem. Phys.* **2004**, *120*, 7741.
(10) Shapovalov, V.; Metiu, H. *J. Catal.* **2007**, *245*, 205.
(11) Camellone, M. F.; Fabris, S. *J. Am. Chem. Soc.* **2009**, *131*, 10473.
(12) Yang, Z.; He, B.; Lu, Z.; Hermansson, K. *J. Phys. Chem. C* **2010**, *114*, 4486.
(13) Nolan, M. *J. Phys. Chem. C* **2009**, *113*, 2425.
(14) Yeriskin, I.; Nolan, M. *J. Chem. Phys.* **2009**, *131*, 244702.
(15) Bueno-Lopez, A.; Krishna, K.; Makkee, M.; Moulijn, J. A. *Catal. Today* **2007**, *121*, 237.
(16) Fierro-Gonzales, J. C.; Gates, B. C. *Catal. Today* **2007**, *122*, 201.
(17) Hernández, W. Y.; Centeno, M. A.; Romero-Sarria, F.; Odriozola, J. A. *J. Phys. Chem. C* **2009**, *113*, 5629.
(18) Patil, S.; Seal, S.; Guo, Y.; Schulte, A.; Norwood, J. *Appl. Phys. Lett.* **2006**, *88*, 243110.
(19) Wang, X.; Rodriguez, J. A.; Hanson, J. C.; Gamarra, D.; Martinez-Arias, A.; Fernandez-Garcia, M. *J. Phys. Chem. B* **2005**, *109*, 19595.
(20) Li, G.; Smith, R. L.; Inomata, H. *J. Am. Chem. Soc.* **2001**, *123*, 11091.
(21) Gupta, A.; Kumar, A.; Waghmare, U. V.; Hegde, M. S. *Chem. Mater.* **2009**, *21*, 4880.
(22) Singh, P.; Hegde, M. S. *J. Solid State Chem.* **2008**, *181*, 3248.
(23) Li, K. Z.; Wang, H.; Wei, Y. G. *J. Phys. Chem. C* **2009**, *113*, 15288.
(24) Kresse, G.; Hafner, J. *Phys. Rev. B* **1993**, *47*, 558.
(25) Kresse, G.; Furthmüller, J. *Phys. Rev. B* **1996**, *54*, 11169.
(26) Blöchl, P. E. *Phys. Rev. B* **1994**, *50*, 17953.
(27) Perdew, J. P.; Burke, K.; Ernzerhof, M. *Phys. Rev. Lett.* **1996**, *77*, 3865.
(28) Perdew, J. P.; Chevary, J. A.; Vosko, S. H.; Jackson, K. A.; Pederson, M. R.; Singh, D. J.; Fiolhais, C. *Phys. Rev. B* **1992**, *46*, 6671.
(29) Perdew, J. P.; Wang, Y. *Phys. Rev. B* **1992**, *45*, 13244.
(30) Monkhorst, H. J.; Pack, J. D. *Phys. Rev. B* **1976**, *13*, 5188.
(31) Nolan, M.; Grigoleit, S.; Sayle, D. C.; Parker, S. C.; Watson, G. W. *Surf. Sci.* **2005**, *576*, 217.
(32) Nolan, M.; Parker, S. C.; Watson, G. W. *Surf. Sci.* **2005**, *595*, 223.
(33) Fabris, S.; de Gironcoli, S.; Baroni, S.; Vicario, G.; Balducci, G. *Phys. Rev. B* **2005**, *71*, 041102.
(34) Fabris, S.; Vicario, G.; Balducci, G.; de Gironcoli, S.; Baroni, S. *J. Phys. Chem. B* **2005**, *109*, 22860.
(35) Dudarev, S. L.; Botton, G. A.; Savrasov, S. Y.; Humphreys, C. J.; Sutton, A. P. *Phys. Rev. B* **1998**, *57*, 1505.
(36) Chen, H.-T.; Choi, Y. M.; Liu, M.; Lin, M. C. *ChemPhysChem* **2007**, *8*, 849.
(37) Loschen, C.; Carrasco, J.; Neyman, K. M.; Illas, F. *Phys. Rev. B* **2007**, *75*, 035115.
(38) Andersson, D. A.; Simak, S. I.; Johansson, B.; Abrikosov, I. A.; Skorodumova, N. V. *Phys. Rev. B* **2007**, *75*, 035109.
(39) Chen, H.-L.; Chang, J.-C.; Chen, H.-T. *Chem. Phys. Lett.* **2011**, *502*, 169.
(40) Chen, H.-T.; Chang, J.-C. *J. Chem. Phys.* **2010**, *132*, 214702.
(41) Jiang, Y.; Adams, J. B.; Schilfgaarde, M. V. *J. Chem. Phys.* **2005**, *123*, 064701.
(42) Hill, S. E.; Catlow, C. R. A. *J. Phys. Chem. Solids* **1993**, *54*, 411.
(43) Kummerle, E. A.; Heger, G. *J. Solid State Chem.* **1999**, *147*, 485.
(44) Skorodumova, N. V.; Ahuja, R.; Simak, S. I.; Abrikosov, I. A.; Johansson, B.; Lundqvist, B. I. *Phys. Rev. B* **2001**, *64*, 115108.
(45) Yang, Z. X.; Woo, T. K.; Baudin, M.; Hermansson, K. *J. Chem. Phys.* **2004**, *120*, 7741.
(46) Lyons, D. M.; Ryan, K. M.; Morris, M. A. *J. Mater. Chem.* **2002**, *12*, 1207.
(47) Lyons, D. M.; McGrath, J. P.; Morris, M. A. *J. Phys. Chem. B* **2003**, *107*, 4607.
(48) Mills, G.; Jönsson, H.; Schenter, G. *Surf. Sci.* **1995**, *324*, 305.
(49) Henkelman, G.; Uberuaga, B. P.; Jönsson, H. *J. Chem. Phys.* **2000**, *113*, 9901.
(50) Yang, Z.; Woo, T. K.; Hermansson, K. *Chem. Phys. Lett.* **2004**, *396*, 384.
(51) Liu, T.; Guo, L.; Tao, Y.; Hu, T. D.; Xie, Y. N.; Zhang, J. *Nanostruct. Mater* **1999**, *11*, 1329.
(52) Pozdnyakova, O.; Teschner, D.; Kröhnert, J.; Jentoft, F. C.; Knop-Gericke, A.; Schlögl, R.; Wootsch, A. *J. Phys. Chem. C* **2007**, *111*, 5426.
(53) Li, C.; Sakata, Y.; Arai, T.; Domen, K.; Maruya, K.; Onishi, T. *J. Chem. Soc., Faraday Trans. 1* **1989**, *85*, 929.
(54) Li, C.; Sakata, Y.; Arai, T.; Domen, K.; Maruya, K.; Onishi, T. *J. Chem. Soc., Faraday Trans. 1* **1989**, *85*, 1451.
(55) Herschend, B.; Baudin, M.; Hermansson, K. *Chem. Phys.* **2005**, *328*, 345.